THE BALTIC JOURNAL
OF ROAD AND BRIDGE ENGINEERING

2010
5(4): 207–217

LOCAL BUCKLING INFLUENCE ON THE MOMENT REDISTRIBUTION COEFFICIENT FOR COMPOSITE CONTINUOUS BEAMS OF BRIDGES

Samy Guezouli[1], Mohammed Hjiaj[2], Nguyen Quang Huy[3]

National Institute of Applied Sciences INSA, 20 Av. des Buttes de Coësmes 35043, Rennes, France
E-mails: [1]samy.guezouli@insa-rennes.fr; [2]mohammed.hjiaj@insa-rennes.fr;
[3]quang-.huy.nguyen@ens.insa-rennes.fr

Abstract. The present paper is concerned with the elastic design optimisation of continuous composite beams. This optimisation is based on the analysis of the beam in the inelastic range including the concrete creep and shrinkage, the tension stiffening and temperature difference effects as well as the possible local buckling instability. The finite element program PONTMIXTE (adapted to study continuous beams at real scale with short time computation) is first presented with its different sections: Pre-design (in accordance with Eurocode specifications), Non linear finite element calculation and Post-processing. In order to validate the proposed model, the numerical calculations are compared against experimental results from tests on a two-span beam in reduced scale (7.5 m length for each span) without taking into account the local buckling phenomenon avoided in the experimental test by using web-stiffeners. Next, special attention is paid to study the influence of the local buckling instability on the internal moment redistribution coefficient between hogging and sagging zones. The application concerns different 3-span beams of bridge at real scale with medium span lengths (40–60–40 m). The post-buckling behaviour represented by moment-rotation curves (M-θ) is deduced from a 3D finite element model of the cross-section developed using Castem finite element code. The M-θ curves describing the local buckling phenomenon are approximated using hyperbolic functions and implemented in PONTMIXTE using a specific rotational spring finite element. The influence of this instability on the moment redistribution coefficients calls the Standart predictions into question.

Keywords: Eurocode, bridges, finite element model (FEM), composite beams, local buckling, moment redistribution.

1. Introduction

Steel-concrete composite structures are common practice today in bridges and industrial buildings. The advantages of both materials lead to a very economic alternative especially in terms of high bearing capacity. The Structural Laboratory of INSA, Rennes, France has performed some experimental tests including one of a two-span beam that will be used to valid the finite element model PONTMIXTE (Guezouli, Yabuki 2006). Depending on the hogging cross-section class, the *prEN 2003 – Eurocode 4: Design of Composite Steel and Concrete Structures – Rules for Bridges – Part 2, Stage 34 Draft Revised,* give the max moment redistribution coefficient allowed in the case of cracked or uncracked elastic global analyses, so the knowledge about the influence of some phenomena in the inelastic range on the proposed values can reduce significantly the costs. The focus is on the relative less resistant classes of cross-sections that require an Elastic Global Analysis (EGA). The local buckling begins generally before reaching the elastic bending resistance for class 4 and between elastic and plastic resistances for class 3. Experimental and finite element (FE) studies on the local buckling of steel girders have been described in many papers (Davies, Mandal 1979; Shanmugam, Wan Mohtar 2007; Škaloud, Rokey 1972; Žilinskaitė, Žiliukas 2009) and the elastic as well as the inelastic behaviour of plate girders having uniform cross-section along the beam is well understood. Without taking into account a specific classification of these cross sections, Škaloud and Rokey (1972) concluded that the ultimate load carrying capacity is influenced by the flexural rigidity of the flanges for girders having similar proportions to those employed in civil engineering construction. Porter *et al.* (1975) assumed that the failure will occur when a certain region of the web yields as a result of the combined effect of the inclined tensile membrane stress field and the web buckling stress. So, it appears that the combined rigidity of compressed flange and the web, for a steel panel under negative bending moment, remains the first parameter influencing the load carrying capacity of the cross-section.

ISSN 1822-427X print / ISSN 1822-4288 online
doi: 10.3846/bjrbe.2010.29
http://www.bjrbe.vgtu.lt

2. The model PONTMIXTE

The main item of PONTMIXTE software includes a graphical post-processor PMIXTPOST for plotting needed variable all along the beam or against the increasing load (Guezouli, Aribert 2001). The continuous beam could be pre-designed with constant cross-section along the beam (for buildings) or different flange thicknesses on hogging zone than those in sagging zone (for bridges) (Brozzetti 2000). The algorithm select the most critical loading cases on hogging and sagging zones between the possible ones (example: for a two-span beam, 4 possible loading cases for asymmetrical beams reduced to 2 cases for symmetrical ones if both distributed and concentrated variable loads could be applied to the beam). In the case of class 3 or 4 cross-sections on hogging zone, the unknown values of bottom flange thicknesses could be found by an iterative process balanced between two critical loading cases:

- critical loading case in sagging zone: max moment close to the plastic resistant moment;
- critical loading case on hogging zone: max moment close to the elastic resistant moment.

Different FE models of composite beams have been proposed (Chung, Sotelino 2006; Guezouli, Aribert 2001; Nguyen *et al.* 2008). Fig. 1 presents the finite element model (FEM) used in the program PONTMIXTE. This model considers a reinforced concrete slab connected to a steel girder. The composite beam FE (node *i* to node *j*) has 4 degrees of freedom per node:

$$\{d_e\} = \{u_i^{(c)} \quad u_i^{(a)} \quad v_i \quad \theta_i \quad u_j^{(c)} \quad u_j^{(a)} \quad v_j \quad \theta_j\}^t. \quad (1)$$

For the node "*i*" for example (Fig. 2), the longitudinal displacements are: $u_i^{(c)}$ for the concrete slab and $u_i^{(a)}$ for the steel girder applied at each corresponding centroid, the vertical displacement v_i and the rotation θ_i both applied at the neutral axis of the entire composite cross-section. The stud slip is defined by:

$$\gamma_i = u_i^{(c)} - u_i^{(a)} + d \times \theta_i, \quad (2)$$

where d – the distance between the slab and the girder neutral axis.

The slab is connected to the steel beam by 2 springs at both ends.

First numerical integration is performed along the element (2 Gauss points) and the second one concerns each fibre constituting the entire composite cross-section (Fig. 2a). Non linear equations are solved using a step-by-step method including a secant algorithm. The automatic longitudinal mesh of the beam could be in accordance with the connection distribution or not. Along the beam, 5 Gauss points are necessary in the variable part of the beam (slope 25%) and 2 Gauss points are enough elsewhere (Fig. 2b).

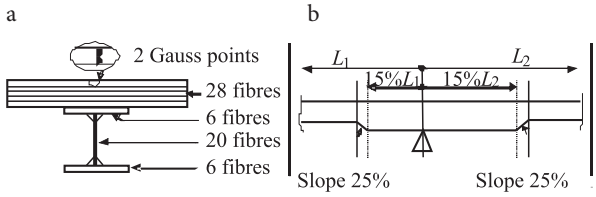

Fig. 2. Cross-section integration (a); variable inertia (b)

The calculation keep running until the imposed stopping calculation (such as reaching the elastic moment at intermediate support, or application of the whole defined loads etc.). This generally occurs before anyone of the following material failure criteria is reached:

- max compression in the concrete slab;
- max strain in the steel girder;
- max strain in the reinforcing steel;
- max slip of the stud.

The convergence of the iterative process is tested on the norm of the displacements limited to 10^{-4}.

The symmetrical stiffness matrix of the composite beam element (*ij*) including a stud at the node "j" for example, is presented in Eq (3) with the following notation:

$k_{ij}^{(c)}$ – the *ij* value in the concrete stiffness matrix (6×6);

$k_{ij}^{(a)}$ – the *ij* value in the girder stiffness matrix (6×6);

R_{ij} – the *ij* value in the stud stiffness matrix (3×3).

The specific FE for local buckling instability (Fig. 3) includes longitudinal displacements for the concrete slab and the girder connected to a rotational spring. The Moment-Rotation curve (M–θ) describing the local buckling will be followed as soon as the point (M_v, θ_v) is reached. This point represents the beginning of the buckling and will be numerically established. The secant stiffness of the buckling FE can be easily added at appropriate degrees of freedom in Eq (3).

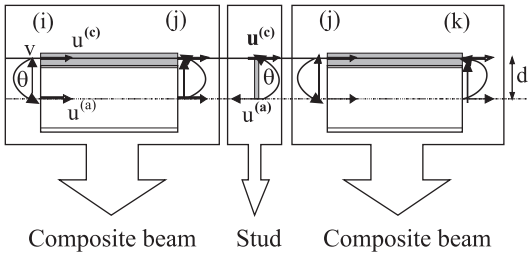

Fig. 1. Composite beam FE

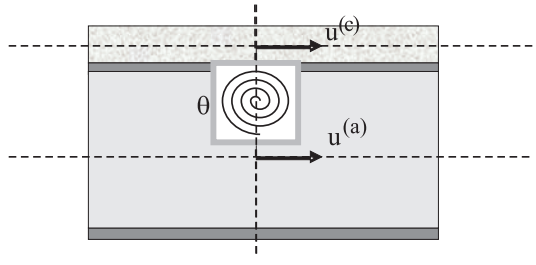

Fig. 3. Local buckling element with rotational spring

$$[K]=\begin{bmatrix} k_{11}^{(c)} & 0 & k_{12}^{(c)} & k_{13}^{(c)} & k_{14}^{(c)} & 0 & k_{15}^{(c)} & k_{16}^{(c)} \\ & k_{11}^{(a)} & k_{12}^{(a)} & k_{13}^{(a)} & 0 & k_{15}^{(a)} & k_{16}^{(a)} & k_{16}^{(a)} \\ & & (k_{22}^{(c)}+k_{22}^{(a)}) & (k_{23}^{(c)}+k_{23}^{(a)}) & k_{24}^{(c)} & k_{24}^{(a)} & (k_{25}^{(c)}+k_{25}^{(a)}) & (k_{26}^{(c)}+k_{26}^{(a)}) \\ & & & (k_{33}^{(c)}+k_{33}^{(a)}) & k_{34}^{(c)} & k_{34}^{(a)} & (k_{35}^{(c)}+k_{35}^{(a)}) & (k_{36}^{(c)}+k_{36}^{(a)}) \\ & & & & (k_{44}^{(c)}+R_{11}) & R_{12} & k_{45}^{(c)} & (k_{46}^{(c)}+R_{13}) \\ & & & & & (k_{44}^{(a)}+R_{22}) & k_{45}^{(a)} & (k_{46}^{(a)}+R_{23}) \\ & & & & & & (k_{55}^{(c)}+k_{55}^{(a)}) & (k_{56}^{(c)}+k_{56}^{(a)}) \\ Sym. & & & & & & & (k_{66}^{(c)}+k_{66}^{(a)}+R_{33}) \end{bmatrix}. \quad (3)$$

3. Material behaviours

The curves describing the material behaviour of each component are shown in Fig. 4 using following Eqs (4)–(5):

Concrete: $$\frac{\sigma^{(c)}}{f_{cm}}=\frac{k\eta-\eta^2}{1+(k-2)\eta} \quad (4)$$

with: $\eta=\frac{\varepsilon^{(c)}}{\varepsilon_m}>0$ and $k=1.1E_{cm}\frac{\varepsilon_m}{f_{cm}}$

Stud: $$Q=Q_u\left(1-e^{-c_1|\gamma|}\right)^{c_2} \quad (5)$$

The parameters c_1 and c_2 (Eq (5)) depend on the ductility of the stud and can be easily obtained using a push-out test; usual values are: $c_1 = 0.7$ and $c_2 = 0.8$.

In order to take into account the creep effect (Fig. 4d), the elastic modulus of the concrete is reduced to $E^{(c)}=\frac{E^{(a)}}{n}$, where $E^{(a)}$ – the usual elastic modulus of structural steel; n – the modular ratio (for first steps loading: $n = \infty$, when the concrete slab is dry: $n = 18$ and leads to: $n = 6$). The temperature difference effect is considered by a superposition of a tension N_{sh} in the concrete slab and a compression in the neutral axis of the composite cross-section (homogenised with $n = 12$) with: $N_{sh}=\frac{\varepsilon_{sh}^{\infty}A^{(c)}E^{(a)}}{n}$ and $M_{sh} = N_{sh} \times x_{sh}$. If the temperature difference between slab and steel girder is about ±5 °C, the total shrinkage including the temperature effect for usual concrete can vary from $\varepsilon_{sh}^{\infty}=3.5\times10^{-4}$ (dry environment) to $\varepsilon_{sh}^{\infty}=2.5\times10^{-4}$ (most favourable environment). The tension stiffening effect is computed in PONTMIXTE as it is defined in *prEN 2003 – Eurocode 4.*

4. Finite element model validation

The pre-design algorithm leads to a hogging cross-section of class 3 (Fig. 5).

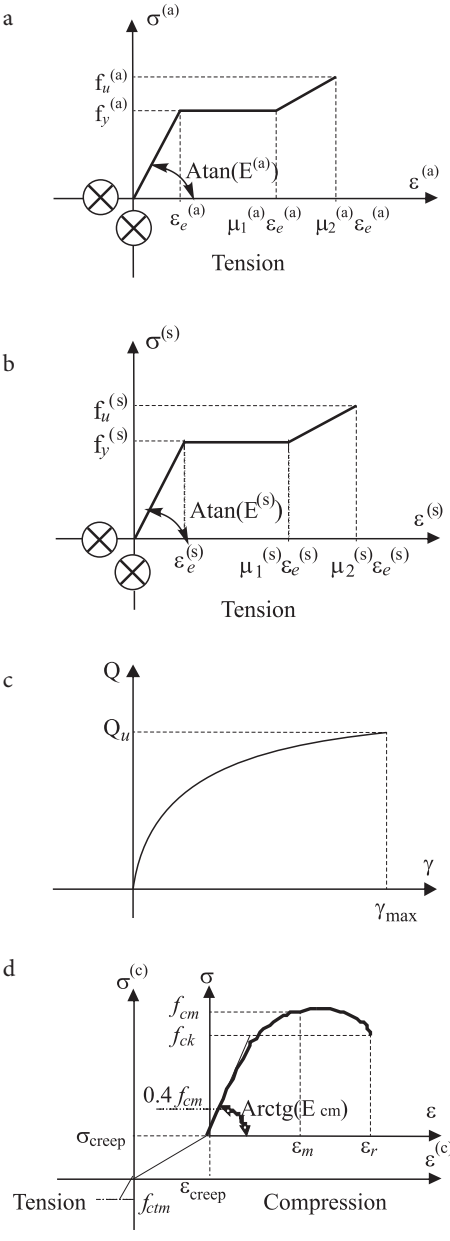

Fig. 4. Steel girder behaviour (a); reinforcing steel behaviour (b); ductile stud behaviour (c); concrete behaviour with creep (d)

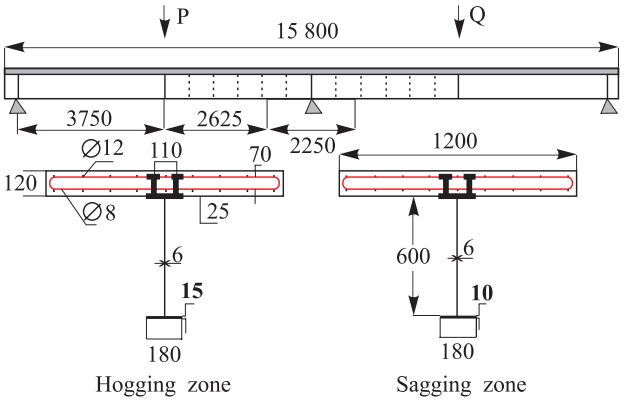

Fig. 5. Geometrical characteristics of the twin-beam

In sagging zones, the cross-section is assumed to be of class 1 because the slab is fully connected to the girder. An uncracked elastic global analysis is performed. The self weight is taken into account (4.17 kN/m for sagging zones and 4.26 kN/m for hogging ones). Only concentrated loads are applied on the beam, a load P applied at the left mid-span increases proportionally to a load Q applied at the right mid-span. For the first critical loading case (the one concerning the sagging zone), only P is applied and for the second critical loading case (the one concerning the hogging zone), both P and Q are applied proportionally. It is assumed that the hogging zone concerns 15% of the span length on each side of the intermediate support. For this zone, the pre-design algorithm proposes 15 mm for the bottom flange thickness while for other cross-sections in sagging zones only 10 mm are required. The top flange thickness is equal to the bottom one. After the beam predesign, a non linear calculation is carried out with the following loading history: the load P applied at the left mid-span increases proportionally to the load Q applied at the right mid-span until 550 N. At this load level, Q remains constant and P still increases until one of the failure criteria described above is reached. Mechanical characteristics are summarised in Table 1. Figs 6, 7 respectively, show that the comparison between numerical and experimental results is satisfactory both for deflection (unfortunately the measurements under the load Q have not been done), and for the bending moment under the load P at the intermediate support. Numerical and experimental failures are reached by concrete cracking under the load P for $P + Q \approx$ 1400 kN giving:

– max displacement under P:

$$w_{\max}^{experimental} = 48 \text{ mm}; \; w_{\max}^{numerical} = 45 \text{ mm},$$

– max moment at intermediate support:

$$M_{\max}^{-experimental} = 960 \text{ kNm}; \; M_{\max}^{-numerical} = 963 \text{ kNm},$$

– max moment under P:

$$M_{\max}^{+experimental} = 1140 \text{ kNm}; \; M_{\max}^{+numerical} = 1130 \text{ kNm}.$$

Table 1. Mechanical characteristics

Material	Parameters values
Slab	$E_{cm} = 36\,000$ MPa, $f_{ck} = 40$ MPa, $f_{cm} = 48$ MPa, $f_t = 2$ MPa, $\varepsilon_m = 0.0022$, $\varepsilon_r^{(c)} = 0.004$
Girder	$E^{(a)} = 190\,000$ MPa, $f_y^{(a)} = 475$ MPa, $f_u^{(a)} = 620$ MPa, $\mu_1^{(a)} = 10$, $\mu_2^{(a)} = 28$
Bars	$E^{(s)} = 200\,000$ MPa, $f_y^{(s)} = 443$ MPa, $f_u^{(s)} = 565$ MPa, $\mu_1^{(s)} = 1$, $\mu_2^{(s)} = 32$, $\varepsilon_u^{(s)} = \mu_2^{(s)} \varepsilon_e^{(s)}$
Stud	$Q_u = 80\,000$ N, $c_1 = 0.7$, $c_2 = 0.8$, $\gamma_{\max} = 6$ mm

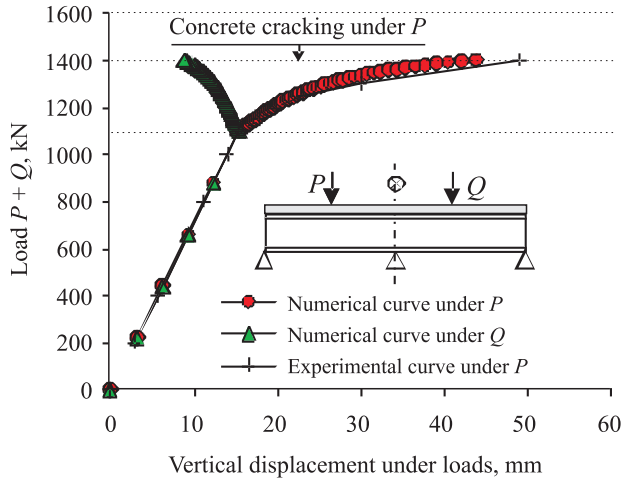

Fig. 6. Comparison of deflections

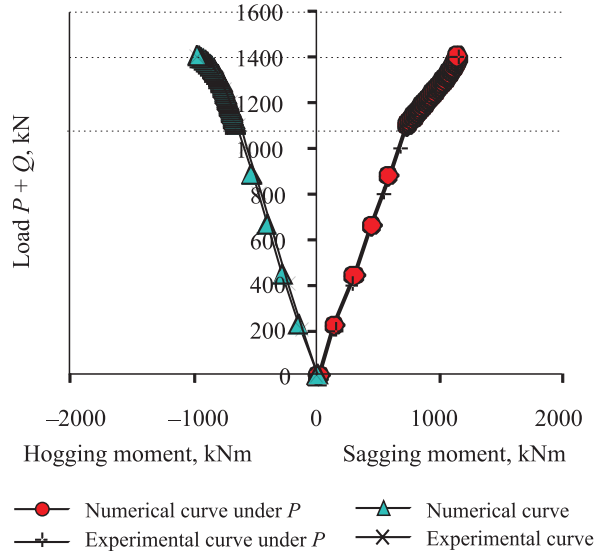

Fig. 7. Comparison of bending moments

It is worth mentioning that the real conditions of the specimen test where considered in this numerical simulation taking into account the tension stiffening, the concrete creep and shrinkage as well as the temperature difference effect. Without these options, the results could not be as close as those obtained (Guezouli, Aribert 2004). This

validation does not include the local buckling phenomenon because the concrete cracking (max compression) occurred before as the failure criterion. For this reason, the simulation of a continuous beam at real scale with hogging cross-sections of class 3 or 4 appears necessary to simulate the local buckling using the specific FE previously defined in Fig. 3.

5. Influence of local buckling on the moment redistribution for a continuous beam at real scale

Firstly, the pre-design of the 3-span beam leads to a hogging cross-section of class 3 and a bottom flange as well as the web of class 3. Mechanical characteristics are given in Table 2. For reminder, the whole cross-section class is the max one between the compressed flange and the web. Table 3 shows different cross-sections provided for by this investigation taking care to be always in the case of a girder cross-section of class 3. The cross-section obtained by the pre-design is noted H5. It represents the less resistant one by comparison to the other ones (H1 to H4) for which the thicknesses were arbitrarily increased or decreased in order to vary the classes of the bottom flange and the web from class 1 to 3. It should be noted that the flange thicknesses in sagging zones remain the same for all the beams, the web thickness is constant all along each beam, the self-weight of the girder becomes different from one beam to another and the critical position of concentrated variable loads Q is the same for all the beam in the case of type A (symmetrical loading case) and supposed the same in the case of type B (asymmetrical loading case) (Fig. 8). It is pointed out that only the pre-designed beam remains optimized at ultimate and serviceability limit states (ULS and SLS). Geometrical characteristics of hogging cross-sections are given in Table 4 with also some arbitrary modifications proposed for the web and the bottom flange giving always a girder cross-section of class 4 on hogging.

Table 2. Mechanical characteristics

Material	Parameters values
Slab	E_{cm} = 35 000 MPa, f_{ck} = 40 MPa, f_{cm} = 48 MPa, f_t = 3.5 MPa, ε_m = 0.0025, $\varepsilon_r^{(c)}$ = 0.0035
Girder	$E^{(a)}$ = 210 000 MPa, $f_y^{(a)}$ = 355 MPa, $f_u^{(a)}$ = 510 MPa, $\mu_1^{(a)}$ = 10, $\mu_2^{(a)}$ = 25
Bars	$E^{(s)}$ = 200 000 MPa, $f_y^{(s)}$ = 400 MPa, $f_u^{(s)}$ = 432 MPa, $\mu_1^{(s)}$ = 1, $\mu_2^{(s)}$ = 25
Stud	Q_u = 174 900 N, c_1 = 0.7, c_2 = 0.8, γ_{max} = 6 mm

The traffic loads applied to the bridge (here a twin-steel girder bridge) have values in accordance with the Model 1 (*EN 1991-2:2002. Eurocode 1: Actions on Structures. General Actions. Actions on Structures Exposed to Fire*) namely a "U.D.L." of 9 kN/m^2 for the lane 1 and 2.5 kN/m^2 for the lanes 2 and 3, and a Tandem System with 2 axle loads each equal to 300 kN. In the transverse direction the traffic loads are distributed according to a linear influence line. Finally, the numerical characteristic values of traffic loads for the most loaded lane are: q = 31.2 kN/m and $Q1 = Q2$ = 406 kN (with the distance 1200 mm).

5.1. A 3D finite element model for buckling analysis

The 3D model (Fig. 9) developed on the finite element code Castem represents the steel girder as well as the stiffeners meshed by 4-nodes shells, the studs are meshed using 3D beams to ensure the displacements continuity with the shells (same degrees of freedom) and the reinforcing bars are replaced by equivalent shells supposed at the top of the

Table 3. Cross-sections under investigation on hogging zone – class 3

Cross-section	Web thickness, mm	Web class	Bottom flange thickness, mm	Bottom flange class
H1	30	1	50	3
H2	25	2	50	3
H3	20	3	60	1
H4	20	3	55	2
H5	20	3	50	3

Table 4. Cross-sections under investigation on hogging zone – class 4

Cross-section	Web thickness, mm	Web class	Bottom flange thickness, mm	Bottom flange class
K1	30	1	35	4
K2	25	2	35	4
K3	20	3	35	4
K4	15	4	60	1
K5	15	4	55	2
K6	15	4	50	3
K7	15	4	35	4

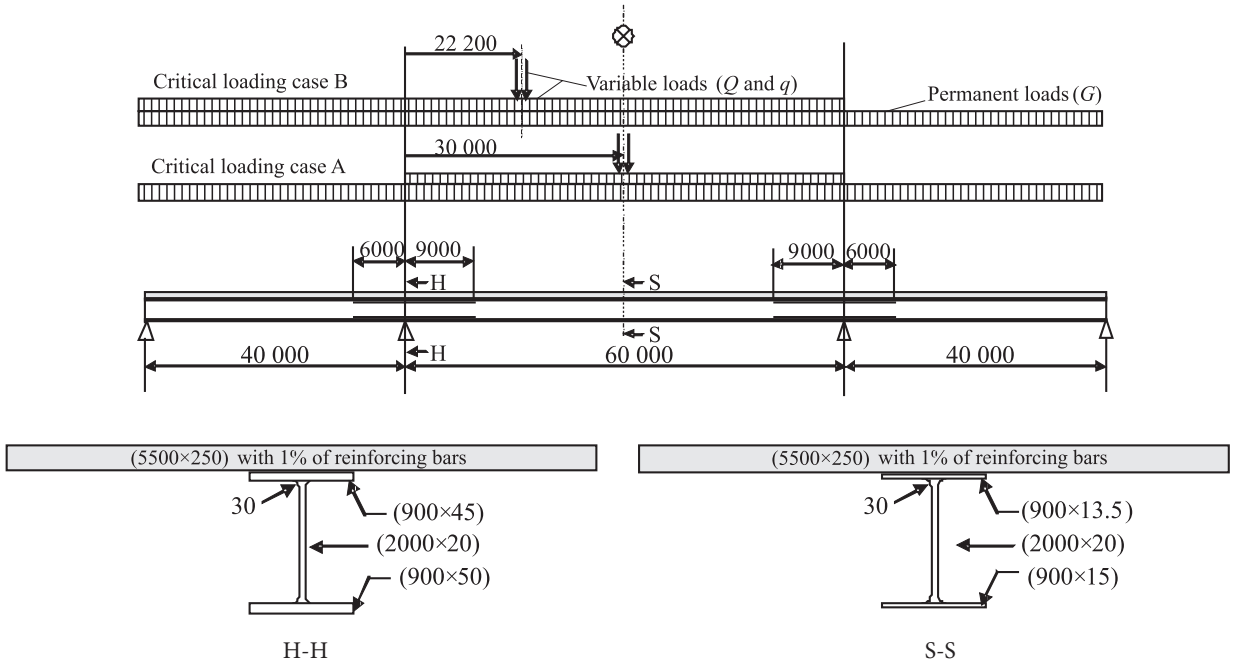

Fig. 8. Pre-design results and critical loading cases

studs. The panel length is equal to twice the web height (h_w) beginning from the cross-section H-H. For boundary conditions (Fig. 9), A and B (top flange and bars), the lateral displacement U_{yy} is equal to zero all along the X axis. For the bottom flange (C), with same conditions, the curve (M-θ) concerns only local buckling otherwise it may include also the lateral tortional buckling. It is supposed that on hogging zone the concrete slab is totally cracked so it does not need to be meshed. Nevertheless, very stiff springs should be represented to keep same distance between the top flange of the girder and the reinforcing bars during the loading. It's pointed out that the springs have no influence on the shear behavior of the studs (Faella *et al.* 2002; Guezouli *et al.* 2008). This simplification requires common mesh nodes between the studs and the reinforcing bars.

The comparison of the transverse displacements of the web at ultimate limit state (Fig. 10) shows clearly that the addition of very stiff spring elements to the model has a negligible influence on the mechanical behaviour and the studs appear working exclusively in shear. The model is loaded by applying a displacement at its end to avoid possible geometrical element distortion. The vertical displacement U_z equal to 200 mm is applied in 10 steps. The curves (M-θ) are plotted for different cross-sections of class 3 (Fig. 11) and of class 4 (Fig. 12). The rotation capacity of the cross-section is similar for all the cross-sections. The max point of each curve represents the beginning of the local buckling (M_v, θ_v). After this point, a hyperbolic decreasing model (Eq (6)) could be adopted with appropriate values for M_0, M_v and θ_v (M_0 represents a horizontal asymptotic line). The web thickness has a stronger influence on these curves than the bottom flange one (on the initial stiffness and also on the max hogging moment). The decreasing curves after buckling is similar with nearly the same value of buckling rotation ($\theta_v \approx 0.014$ rad). The curve related to Eq (6) plotted for H1 as an example, gives a good prediction for the behaviour after buckling. The buckling rotation is also nearly the same in the case of cross-section of class 4 ($\theta_v \approx 0.012$ rad).

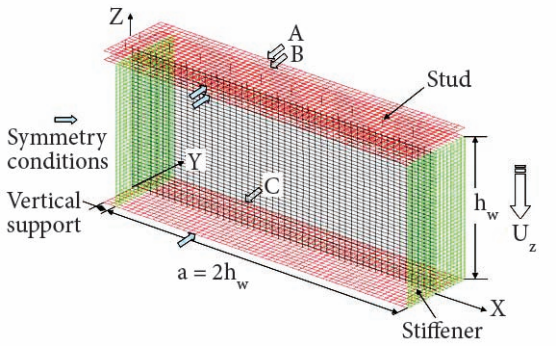

Fig. 9. Simplified 3D model

$$M = M_0 + \left(M_v - M_0\right)\frac{\theta_v}{\theta}, \quad \forall\theta \geq \theta_v. \tag{6}$$

Remarks:

Before setting about a non-linear stability calculation, a linear stability one is carried out and the whole displacement field is reduced by a scale of 5% in the aim to represent an initial deformation of the specimen (initial deformation data for non-linear calculation).

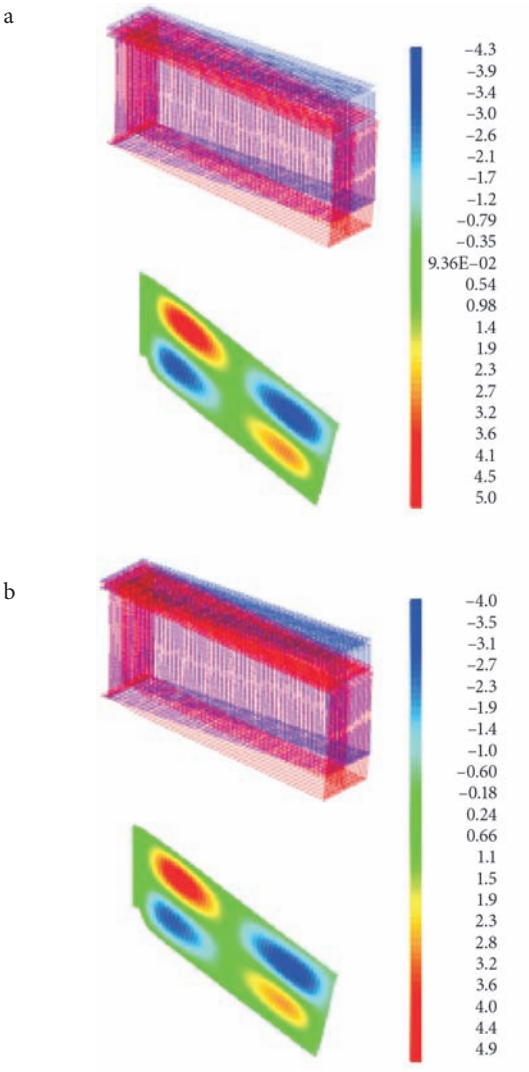

Fig. 10. Without springs (a); with springs (b)

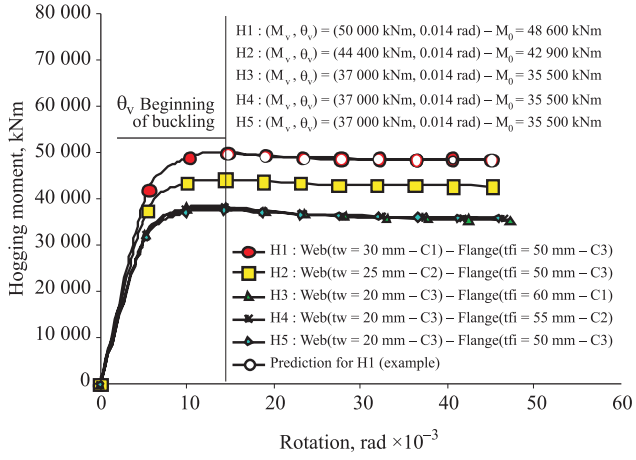

Fig. 11. 3D calculations and buckling curves – class 3

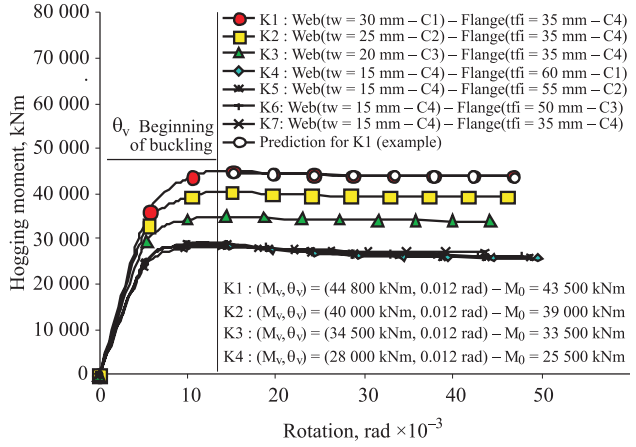

Fig. 12. 3D calculations and buckling curves – class 4

There is no significant sense to talk about available rotation capacity at the intermediate support for cross-sections of classes 3 and 4 because of the local buckling.

5.2. Results of the numerical analysis

The moment redistribution coefficient (%) is calculated with the Eq (7):

$$R = \frac{\left|M_{Ed.Rd}^{-(uncr)} - M_{1+2}^{-}\right| - \left|M_{el.Rd}^{-(num)} - M_{1+2}^{-}\right|}{\left|M_{Ed.Rd}^{-(uncr)} - M_{1+2}^{-}\right|} \times 100, \quad (7)$$

where $M_{Ed.Rd}^{-(uncr)}$– the hogging moment obtained by a virtual elastic calculation (using the same loading level λ); $M_{el.Rd}^{-(num)}$ – the numerical hogging moment obtained for H-H cross-section; M_{1+2}^{-}– the hogging moment resulting only from the first and second loading steps corresponding respectively to the selfweight of the girder and the one of the concrete that is still wet (Guezouli, Aribert 2004; Guezouli 2007; Guezouli, Yabuki 2008). During these steps, the cross-section is not considered resisting as a composite cross-section so, this part of bending moment must be subtracted to the ones defined previously. The proposed hyperbolic model has been implemented in the program PONTMIXTE and different simulations are carried out with appropriate values of the model parameters (M_0, M_ν and θ_ν). The calculation termination criterion is either reaching the plastic resistant moment in sagging zone (generally occurs for the critical loading case of type A) or the elastic moment resistant at the intermediate support (generally occurs for the critical loading case of type B).

5.2.1. Results for the beams of class 3

Different values of the variables involved in Eq (7) without and with taking into account possible local buckling are given in Tables 5 and 6, respectively. The variation of the hogging moment against the cumulative load (Figs 13, 14, 15), show that for the beams H1 and H2, the elastic resistant moment is reached before the buckling characteristic

point (M_v, θ_v): no influence of local buckling on the moment redistribution coefficient, the cross-sections seams to be relatively resistant. For the beams H3, H4 and H5, without taking into account the local buckling, the rule of 10% redistribution predicted in *ENV 1994-2:1997 Eurocode 4: Design of Composite Steel and Concrete Structures - Part 2: Composite Bridges*, seems to be un-adequate especially for loading case of type A but the occurrence of local buckling decreases the value of the numerical hogging moment increasing consequently the value of the redistribution coefficient *R*. This value becomes finally larger than 10% for both loading cases. Because of local buckling, the calculation stops for lower values of λ ($\lambda^{\text{buckling}} \leq \lambda^{\text{no buckling}}$) especially for loading case of type B and necessary the elastic moment $M_{Ed.Rd}^{-(uncr)}$ changes and, consequently the value of *R*. In the column of λ (Tables 5, 6), the letters correspond to the stopping calculation criterion for each beam [(A) → $M_{pl.Rd}^{+}$ and (B) → $M_{el.Rd}^{-}$]. It must be noted that the beams H1 and H4 have been arbitrary defined on hogging zone stronger than the one obtained by the pre-design optimization (H5). This leads necessary to values of $\lambda \geq 1.35$. For example, in the loading case B of the beam H3, the numerical bending moment can be plotted along the beam by comparison to the virtual elastic calculation. Without local buckling (Fig. 16a) the elastic hogging bending is obtained while the lower layer of the girder bottom flange reaches its elastic limit (this occurs for $\lambda = 1.60$, value adopted for plotting the curves). It is clear that for this critical loading case, the left intermediate support is mostly concerned with the local buckling compared to the right one (see the dot-line corresponding to buckling moment). If the local buckling is taken into account (Fig. 16b), the same stopping calculation criterion, as the one described before, is reached for a lower loading level ($\lambda = 1.41$). The first element that begins to buckle is located on the left intermediate support causing redistribution of internal forces. Local buckling extends on both sides defining the zone subjected to this instability.

Table 5. Hogging and sagging bending, kNm – see Table 3 (class 3) - all options – local buckling not included

Beams	$M_{el.Rd}^{-(num)}$	$M_{Ed.Rd}^{-(uncr)}$	M_{1+2}^{-}	$M_{pl.Rd}^{-}$	$M_{Sd}^{+(num)}$	$M_{pl.Rd}^{+}$	λ	*R*, %
Loading case of type A (Fig. 9)								
H1	−41 706	−43 653	−17 232	−48 958	37 058	37 563	1.71(B)	7
H2	−39 825	−41 166	−16 987	−47 072	33 374	33 541	1.51(A)	6
H3	−37 698	−39 046	−17 090	−51 843	29 228	29 462	1.35(A)	6
H4	−37 632	−38 712	−16 927	−48 487	29 285	29 462	1.35(A)	5
H5	−37 556	−38 340	−16 745	−45 150	29 350	29 462	1.35(A)	4
Loading case of type B (Fig. 9)								
H1	−41 722	−47 264	−17 232	−48 958	32 472	37 563	1.54(B)	18
H2	−40 529	−45 027	−16 987	−47 072	29 742	33 541	1.40(B)	16
H3	−45 685	−49 123	−17 090	−51 843	28 872	29 462	1.60(B)	11
H4	−42 460	−45 793	−16 927	−48 487	27 625	29 462	1.42(B)	11
H5	−39 969	−43 146	−16 745	−45 150	26 948	29 462	1.35(B)	12

Table 6. Hogging and sagging bending, kNm – see Table 3 (class 3) – all options – local buckling included

Beams	$M_{el.Rd}^{-(num)}$	$M_{Ed.Rd}^{-(uncr)}$	M_{1+2}^{-}	$M_{pl.Rd}^{-}$	$M_{Sd}^{+(num)}$	$M_{pl.Rd}^{+}$	λ	*R*, %
Loading case of type A (Fig. 9)								
H1	−41 706	−43 653	−17 232	−48 958	37 058	37 563	1.71(A)	7
H2	−39 825	−41 166	−16 987	−47 072	33 374	33 541	1.51(A)	6
H3	−36 379	−39 046	−17 090	−51 843	29 229	29 462	1.35(A)	12
H4	−36 371	−38 712	−16 927	−48 487	29 285	29 462	1.35(A)	11
H5	−36 362	−38 340	−16 745	−45 150	29 350	29 462	1.35(A)	9
Loading case of type B (Fig. 9)								
H1	−41 722	−47 264	−17 232	−48 958	32 472	37 563	1.54(B)	18
H2	−40 529	−45 027	−16 987	−47 072	29 742	33 541	1.40(B)	16
H3	−36 220	−46 051	−17 090	−51 843	28 074	29 462	1.41(B)	34
H4	−36 578	−44 832	−16 927	−48 487	27 335	29 462	1.36(B)	29
H5	−36 746	−43 146	−16 745	−45 150	26 995	29 462	1.35(B)	24

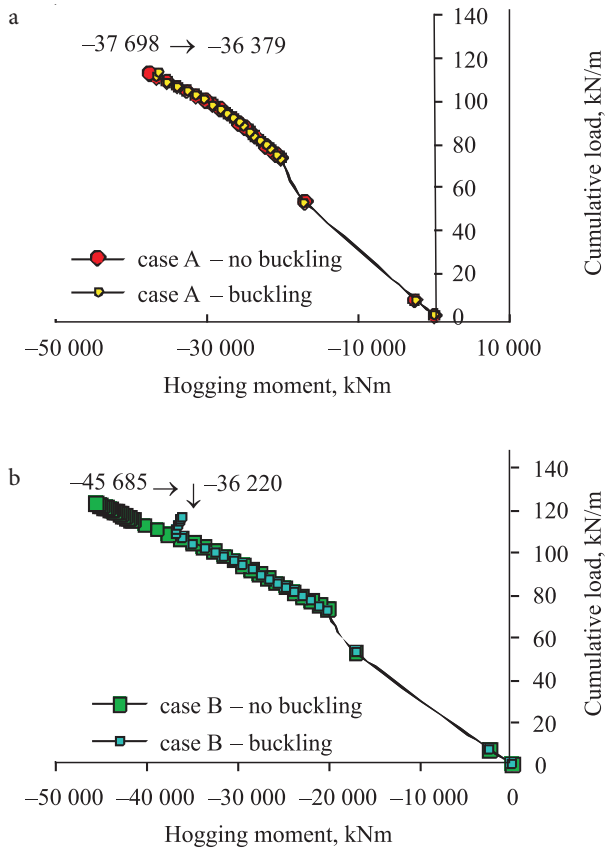

Fig. 13. (θ – M) – bean H3 case A (a) and case B (b)

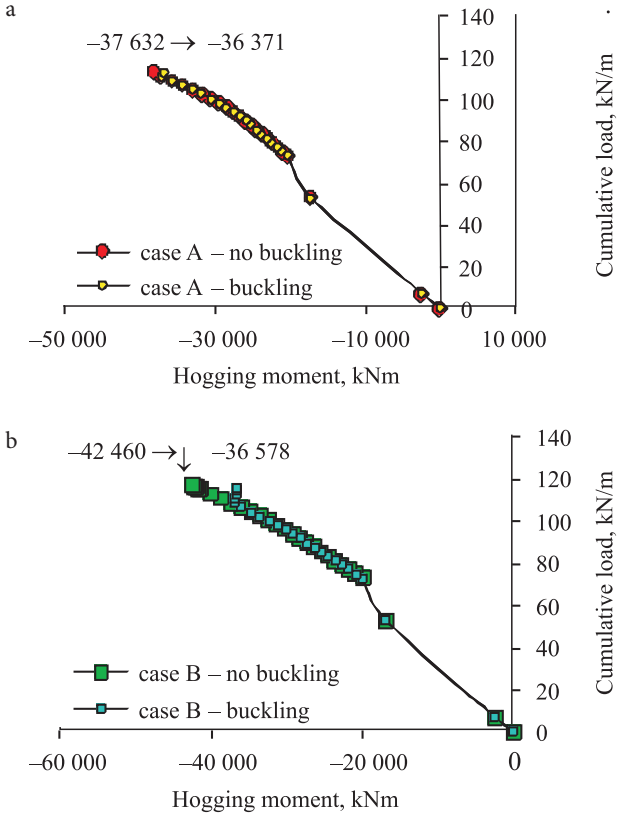

Fig. 14. (θ – M) – bean H4 case A (a) and case B (b)

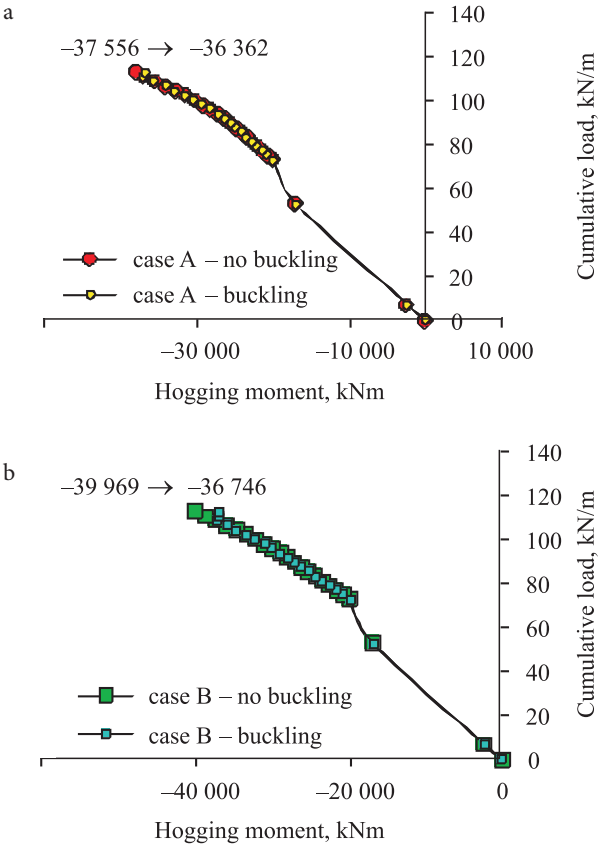

Fig. 15. (θ – M) – bean H5 case A (a) and case B (b)

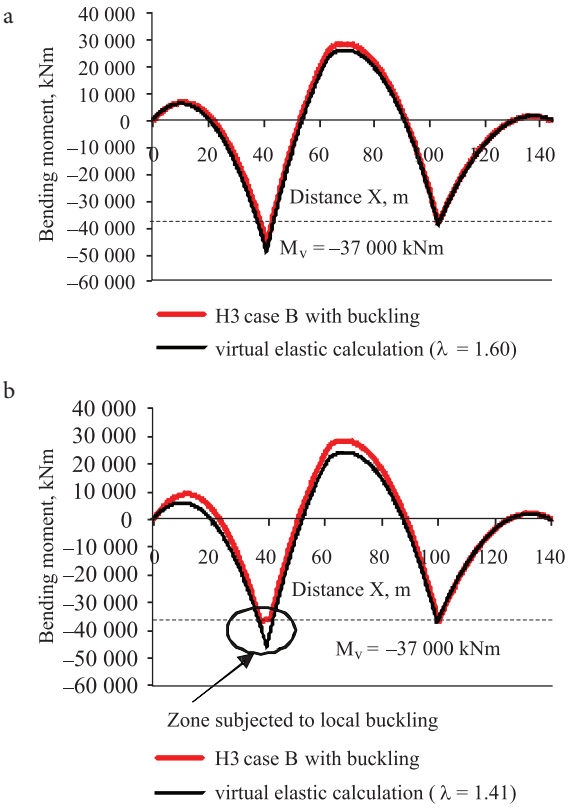

Fig. 16. H3 case B without buckling (a) and H3 case B with buckling (b)

Table 7. Hogging and sagging bending – See Table 4 (class 4) – All options – Local buckling not included

Beams	K1	K2	K3	K4	K5	K6	K7
Loading case of type A (Fig. 9)							
λ	1.35(B)	1.22(B)	1.01(B)	1.22(A)	1.15(A)	1.15(A)	0.81(B)
R, %	24	19	16	2	1	– 0.0	12
Loading case of type B (Fig. 9)							
λ	1.15(B)	1.01(B)	0.88(B)	1.46(B)	1.35(B)	1.15(B)	0.74(B)
R, %	30	28	25	7	8	9	21

Table 8. Hogging and sagging bending (kNm) – See Table 4 (class 4) – All options – Local buckling included

Beams	K1	K2	K3	K4	K5	K6	K7
Loading case of type A (Fig. 9)							
λ	1.35(B)	1.22(B)	1.01(B)	1.15(A)	1.15(A)	1.15(A)	0.81(B)
R, %	24	19	16	53	52	50	20
Loading case of type B (Fig. 9)							
λ	1.15(B)	1.01(B)	0.88(B)	1.35(B)	1.22(B)	1.08(B)	0.74(B)
R, %	30	28	25	67	61	55	29

5.2.2. Results for the beams of class 4

In the case of class 4, Tables 7, 8 summarize only the values of the moment redistribution coefficient. Eq (7) has to be calculated with moments obtained using loads corresponding to the specific value of λ. These values are generally less than 1.35 because most of the beams are less resistant than the pre-designed one. The local buckling appears also more sensible for loading case of type B than the one of type A. Very low values of *R* especially for the loading case A, increases when the local buckling is taken into account. In some cases, *R* could be negative meaning that the redistribution is inverted and happens from mid-spans to intermediate supports. The influence of local buckling on the moment redistribution coefficient appears more important in the case of class 4 than in the case of class 3.

6. Conclusions

This study attempted to show that it is possible to simulate at a real scale the inelastic behaviour of a steel-concrete composite bridge beam with the proposed FE formulation. The comparison of numerical predictions against experimental results for a two-spans beam in reduced scale (half-scale) are good ensuring the ability of FEM to correctly describe the behavior of composite bridges. The main interest concerned the beams with cross-sections of class 3 and 4 in hogging zone that are generally subjected to local buckling. A preliminary study was carried with a 3D FEM to characterize the post-buckling behavior of these cross-section classes. A hyperbolic model was proposed involving three parameters: the buckling point (M_v, θ_v) and the horizontal asymptotic line $M = M_0$. This model was implemented in the code PONTMIXTE and several numerical simulations were carried out to show the significant influence of the local buckling instability on the moment redistribution coefficient from hogging to sagging zones in the case of a 3-span beam bridge at real scale. This influence appears closely linked to the class combination of the compressed flange and the web of the girder. The local buckling mostly occurs when the web is of a higher class (less resistant) than the compressed flange. In this case, if the local buckling is not taken into account, the rule of 10% moment redistribution proposed by the *prEN 2003 – Eurocode 4* becomes inadequate especially for symmetrical loading case. If local buckling is taken into account, the calculation of the moment redistribution coefficient after buckling is the one obtained considering specific constructive measures (web-stiffeners) to avoid local buckling (Fig. 14a). Without stiffeners, no redistribution is allowed for these cross-section classes. kaloud and Zörnerova (2005) paid attention to the post-buckled behaviour and ultimate strength of slender webs; similar approach could be carried out for steel-concrete composite beams and implemented in the code PONTMIXTE. This future prospect could give important information about the influence of the "breathing" web on the moment redistribution coefficient.

References

Brozzetti, J. 2000. Design Development of Steel-Concrete Composite Bridges in France, *Journal of Constructional Steel Research* 55(1–3): 229–243. doi:10.1016/S0143-974X(99)00087-5

Chung, W.; Sotelino, E. D. 2006. Three-Dimensional Finite Element Modeling of Composite Girder Bridges, *Engineering Structures* 28(1): 63–71. doi:10.1016/j.engstruct.2005.05.019

Davies, G.; Mandal, S. N. 1979. The Collapse Behavior of Tapered Plate Girders Loaded within the Tip, *Ice Proceedings* 67(1): 65–80. doi:10.1680/iicep.1979.2317

Faella, C.; Martinelli, E.; Nigro, E. 2002. Steel and Concrete Composite Beams with Flexible Shear Connection: "Exact" Analytical Expression of the Stiffness Matrix and Applications, *Computers and Structures* 80(11): 1001–1009. doi:10.1016/S0045-7949(02)00038-X

Guezouli, S.; Hjiaj, M.; Nguyen, Q. H. 2008. 3-D F. E. Connection Degree in Composite Continuous Beams – Influence on the Bending Moment Capacity, in *The 5th European Conference on Steel and Composite Structures (Eurosteel 2008).* Ed. by Ofner, R.; Beg, D.; Fink, J.; Greiner, R.; Unterweger, H. September 3–5, 2008, Graz, Austria.

Guezouli, S.; Yabuki, T. 2008. Numerical Investigation on Instabilities of Steel-Concrete Composite Cross-Sections, in *Proc of the 5th International Conference on Thin-Walled Structures*, vol. 2. June 18–20, 2008. Brisbane, Australia, 1007–1014.

Guezouli, S. 2007. Local Buckling of Class 4 Cross-Section – Application to a Steel-Concrete Continuous Beam of Bridge at Real Scale, in *Proc of 3rd International Conference on Steel and Composite Structures (ICSCS'07).* 30 July – 1 August, 2007, Manchester, UK. Manchester, 481–487.

Guezouli, S.; Yabuki, T. 2006. "Pontmixte": a User Friendly Program for Continuous Beams of Composite Bridges, in *Proc of the International Colloquium on Stability and Ductility of Steel Structures (SDSS'06)*. September 6–8, 2006, Lisbon, Portugal.

Guezouli, S.; Aribert, J. M. 2004. Numerical Investigation of Moment Redistribution in Continuous Beams of Composite Bridges, in *Proc of the Composite Construction in Steel and Concrete V.* Ed. by Leon, T. R.; Lange, J. Kruger National Park, South Africa. American Society of Civil Engineers, 47–56. doi:10.1061/40826(186)5

Guezouli, S.; Aribert, J. M. 2001. Approche aux éléments finis pour l'étude du comportement des poutres de ponts mixtes à l'échelle réelle, in *XVème Congrès Français de Mécanique* [XVth French Symposium of Mechanics]. September 3–7, 2001, Nancy, France.

Nguyen, Q. H.; Hjiaj, M.; Uy, B.; Guezouli, S. 2008. Nonlinear F. E. Analysis of Composite Beams, in *Proc of the 5th European Conference on Steel and Composite Structures (Eurosteel 2008).* Ed. by Ofner, R.; Beg, D.; Fink, J.; Greiner, R.; Unterweger, H. September 3–5, 2008, Graz, Austria. Brussels: ECCS European Convention for Constructional Steelwork, 405–410.

Porter, D. M.; Rokey, K. C.; Evans, H. R. 1975. The Collapse Behavior of Plate Girders Loaded in Shear, *Journal of Structural Engineering* 53(8): 313–325.

Shanmugam, N. E.; Wan Mohtar, W. H. M. 2007. Experimental and Finite Element Studies on Tapered Steel Plate Girders, in *Proc of the International Conference on Computational Science 2007 (ICSCS-2007)*. 30 July – 1 August, 2007, Manchester, UK. Manchester, 165–170.

Škaloud, M.; Zörnerova; M. 2005. The Fatigue Behaviour of the Breathing Webs of Steel Bridge Girders, *Journal of Civil Engineering and Management* 11(4): 323–336.

Škaloud, M.; Rokey, K. C. 1972. The Ultimate Load Behaviour of Plate Girders Loaded in Shear, *Journal of Structural Engineering* 50(1): 29–47.

Žilinskaitė, A.; Žiliukas, A. 2009. Buckling of Double-T Construction Elements for Bridges in Case of Complicated Loading, *The Baltic Journal of Road and Bridge Engineering* 4(1): 27–30. doi:10.3846/1822-427X.2009.4.27-30

Received 12 February 2009; accepted 4 September 2010